

# On the mechanism of photoinduced dimer dissociation in the plant UVR8 photoreceptor

Alexander A. Voityuk<sup>a,b,1</sup>, Rudolph A. Marcus<sup>c,d,1</sup>, and Maria-Elisabeth Michel-Beyerle<sup>d,e,1</sup>

<sup>a</sup>lnstitució Catalana de Recerca i Estudis Avançats, 08010 Barcelona, Spain; bInstitute of Computational Chemistry, Universitat de Girona, 17071 Girona, Spain; <sup>c</sup>Noyes Laboratory for Chemical Physics, California Institute of Technology, Pasadena, CA 91125-0072; <sup>d</sup>Division of Physics and Applied Physics, School of Physical and Mathematical Sciences, Nanyang Technological University, Singapore 637371; and eDepartment of Chemistry, Technical University of Munich, 85748 Garching, Germany

Contributed by Rudolph A. Marcus, February 20, 2014 (sent for review January 21, 2014)

UV-B absorption by the photoreceptor UV resistance locus 8 (UVR8) consisting of two identical protein units triggers a signal chain used by plants in connection with protection and repair of UV-B induced damage. X-ray structural analysis of the purified protein [Christie JM, et al. (2012) Science 335(6075):1492-1496] [Wu D, et al. (2012) Nature 484(7393): 214-220] has revealed that the dimer is held together by arginine-aspartate salt bridges. In this paper we address the initial processes in the signal chain. On the basis of high-level quantum-chemical calculations, we propose a mechanism for the photodissociation of UVR8 that consists of three steps: (i) In each monomer, multiple tryptophans form an extended light-harvesting system in which the La excited state of Trp233 experiences strong electrostatic stabilization by the protein environment. The strong stabilization singles out this tryptophan to be an efficient exciton acceptor that accumulates the excitation energy from the entire protein subunit. (ii) A fast decay of the locally excited state by charge separation generates the radical ion pair Trp285(+)-Trp233(-) with a dipole moment of ~18 D. (iii) Key to the proposed mechanism is that this large dipole moment drives the breaking of the salt bridges between the two monomer subunits. The suggested mechanism for the UV-B-driven dissociation of the dimer that rests on the prominent players Trp233 and Trp285 explains the experimental results obtained from mutagenesis of UVR8.

ife on earth depends on sunlight that drives energy conversion and signaling processes, however, at the price that its UV fraction may damage DNA. Counteracting this threat, plants respond to UV-B radiation by the photoreceptor UV resistance locus 8 (UVR8) discovered in Arabidopsis thaliana (1). In the presence of UV-B (280-315 nm), the UVR8 protein accumulates rapidly in the cell nucleus (2, 3). Its interaction with other proteins activates gene expression to protect against or repair UV-B-induced damage (4-7). Unlike other photoreceptors in cells, the protein UVR8 exploits the UV-B absorbance of its intrinsic tryptophans rather than that of exogenic chromophores.

The crystal structure of the UVR8 protein (8, 9) revealed that the dimer is held together by salt bridges between the cationic arginine (R) and anionic aspartate (D) or glutamate (E) side chains at the interface between the two subunits. Exposure of UVR8 to UV-B light causes dissociation of the protein into the monomers. This monomerization is universal, because it is observed for the purified protein (8, 9) and in plants and heterologous systems (10). The crystal structure allows one to infer a cooperative role and an interplay of specific tryptophans. It was suggested (11, 12) that excitation of the tryptophan triad W233, W285, and W337 initiates the dissociation of the dimeric photoreceptor and triggers the signal chain used by plants for UV-B protection (10). Subsequent interactions of monomer subunits with other proteins associated with chromatin have been shown to activate transcription of the target genes (2, 13). This basic understanding of the UVR8 photoreceptor has been corroborated further by the spontaneous reassembly of the monomer subunits restoring the homodimer and its UV-B response (14). In recent years a wide spectrum of aspects related to UVR8 function has been addressed in the literature (15, 16). Still, the mechanism that links UV-B absorption to the dissociation of the photoreceptor remains unclear.

Several mechanisms for the photodissociation of UVR8 have been proposed. One of them involves electron transfer from an excited Trp residue to the cationic arginines, which leads to the breaking of one of the salt bridges (8). Another mechanism implies that absorption of UV-B by Trp residues induces destabilization of their interaction with the neighboring arginines, which in turn causes disruption of critical intermolecular hydrogen bonds (9). So far, there are, however, neither experimental nor computational data that support any of these mechanisms.

In this study, we consider mechanistic features underlying the photoinduced dissociation of the UVR8 protein. On the basis of multistate complete active space second-order perturbation theory (MS-CASPT2) calculations, we find that one "special" tryptophan, Trp233, serves as a sink for excitation energy transferred from other tryptophans of the protein. This unique feature rests on the strong electrostatic stabilization of Trp233 in its excited L<sub>a</sub> state by the protein environment. Upon efficient accumulation of UV-B energy at Trp233, a fast decay of this excited state via charge separation generates the charge transfer state Trp285 (+)Trp233(-) with a large dipole moment of ~18 D. We propose that the significant change in the electric field drives the photodissociation of UVR8. Apart from the well-established concepts (17, 18) that salt bridges are broken when conformational changes force the involved residues to move apart, our calculations point to the possibility of a more local mechanism for the

## **Significance**

In contrast to other chromophore/protein systems in photobiology, the UV-B photoreceptor UV resistance locus 8 (UVR8) utilizes tryptophan residues as light absorbers. The initial step of a signaling pathway that ultimately leads to UV-B protection and damage repair in plants is the breaking of salt bridges that stabilize the UVR8 protein consisting of two identical subunits. On the basis of the known X-ray structure and high-level quantum-chemical computations, we propose a mechanism that implies excitation energy transfer to the "special tryptophan" W233 near the monomer interface, followed by the formation of a charge-transfer state involving W233 and W285. In the calculations, the large dipole moment of W233(–)-W285(+) facilitates the breaking of arginine-aspartate salt bridges between the two subunits.

Author contributions: A.A.V. and M.-E.M.-B. designed research: A.A.V. performed research; A.A.V., R.A.M., and M.-E.M.-B. analyzed data; and A.A.V. and M.-E.M.-B. wrote the paper.

The authors declare no conflict of interest

<sup>1</sup>To whom correspondence may be addressed. E-mail: Alexander.voityuk@icrea.cat, ram@ caltech.edu, or mariaelisabeth@ntu.edu.sg.

This article contains supporting information online at www.pnas.org/lookup/suppl/doi:10.

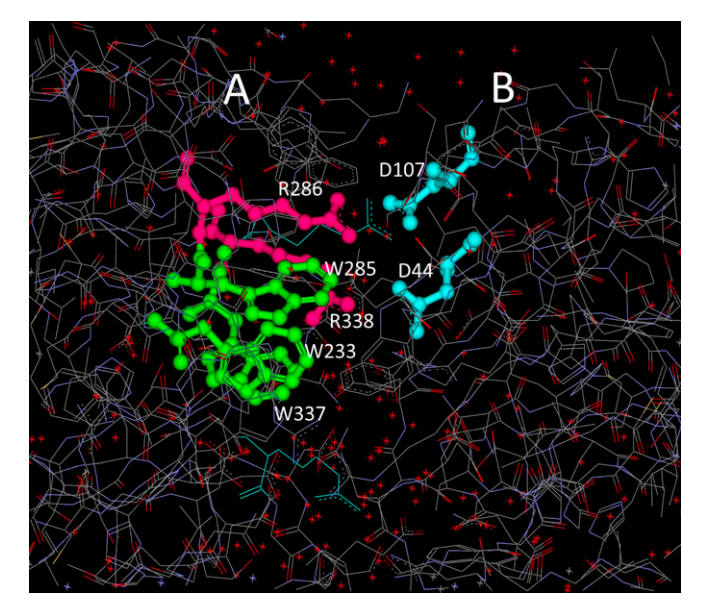


**Fig. 1.** UVR8 X-ray structure. Amino acid residues responsible for photoinduced splitting of the homodimer into the A and B subunits are shown: Trp triad (green) and salt bridges between Arg (pink) and aspartate residues (cyan).

breaking of salt bridges. The changes of the electrostatic potential at the arginines R286 and R338 brought about by the nearby charge transfer (CT) state may facilitate proton transfer between R286 and D96 and lead to the neutral species. Independent of the detailed mechanism of the breaking of salt bridges, the central players are Trp233 and Trp285 and this conclusion is also consistent with the available experimental data (7–10, 19).

## **Results and Discussion**

**Electronic Excitation of Tryptophans in UVR8.** In UVR8 four tryptophan side chains (W94, W233, W285, and W337) located adjacent to salt bridges at the interface between the monomers are arranged in two pyramids across the dimeric interface (Fig. 1). The two subunits of UVR8 are stitched together by several salt bridges: R286-D107, R286-D96, R146-E182, R338-D44, R354-E43, and R354-E53. The importance of such ionic interactions in maintaining the dimeric structure of the UVR8 protein was computationally studied (20).

We first consider the MS-CASPT2 results for the two lowest  $\pi \rightarrow \pi^*$  excitations in the side-chain group of Trp (indole). In Table 1 we compile the computed vertical excitation energies (E), the corresponding wave lengths (L), oscillator strengths (F), dipole moments ( $\mu$ ) in Debye, and the change of the dipole moment upon excitation ( $\Delta \mu_i$ ). The results are in good agreement with previous calculations (21).

Because the dipole moment of indole changes significantly  $(\Delta \mu = 4.2 \ D)$  by the  $L_a$  excitation, the energy of this excited state

Table 1. Excited-state properties of indole calculated with the MS-CASPT2 method, using the ANO-L basis set and the (10, 10) active space

Transition	E, eV	L, nm	F	$ \mu_i $ , D	$ \Delta \mu_i $ , D
L <sub>b</sub>	4.703	264	0.022	1.51	0.49
L <sub>a</sub>	4.887	254	0.121	5.91	4.21

E denotes the excitation energy, L the excitation wavelength, F the oscillator strength,  $\mu_i$  the dipole moment of the excited state, and  $\Delta\mu_i$  the change of the dipole moment upon excitation.

should be sensitive to its local environment. In a polar environment, one observes a red shift of the  $L_a$  absorption bands (22). This shift was estimated from a change in electrostatic interaction of electron density of indole upon vertical excitation.

The stabilization energies were computed using a simple model,  $\Delta = (1/\epsilon) \sum_A \sum_i Q_A ((q_i^{\rm ex} - q_i^0)/R_{Ai})$ , where  $q_i^0$  and  $q_i^{\rm ex}$  are MS-CASPT2 atomic charges of Trp calculated in the ground and excited states, and  $Q_A$  is the charge on the protein atom A obtained using the PDB2PQR program (23).  $R_{Ai}$  is the distance between atoms i and A; only electronic polarization of the environment,  $\epsilon = 2$ , was taken into account, there being no time for relaxation of the protein charges during the absorption event.

As shown in Fig. 2, the L<sub>a</sub> states of the tryptophans are essentially stabilized by residues that belong to the same protein subunit (here to subunit A). The electrostatic interaction with the residues of the subunit B destabilizes the La state of Trps of the subunit A. A similar situation is observed for Trps of the unit B: their L<sub>a</sub> state is stabilized by residues of the same unit, but destabilized by the interaction with the second unit. As also seen in Fig. 2, the interaction with the environment leads to a decrease of the  $L_a$  excitation energy by  $\sim 0.4$  eV; i.e., the calculated absorption maximum is shifted from 254 nm to 280 nm into the region of UV-B radiation. The most important feature is that the electrostatic interaction with the protein matrix stabilizes the L<sub>a</sub> excited state of W233 considerably more than the excited states of other Trp residues. Thus, W233 becomes an efficient exciton acceptor. So the protein makes it energetically favorable for excitons to flow from any other tryptophan in the photoreceptor to the tryptophan at the position 233. The residues D129 and R234 give the largest contribution (-0.51 eV and −0.28 eV, respectively) to the stabilization energy of the L<sub>a</sub> state of W233. More details are given in Table S1. Our estimate of the electrostatic interaction of the electron density in the ground state and the L<sub>b</sub> excited state of Trp with the protein environment shows that the excitation energy of Trps remains almost constant; typically the changes are smaller than 0.05 eV.

**Excitation Energy Transfer Between Tryptophans.** As described in *Methods*, the excitation energy transfer (EET) rate between the Trp residues in the homodimer (Fig. 3) is determined by the

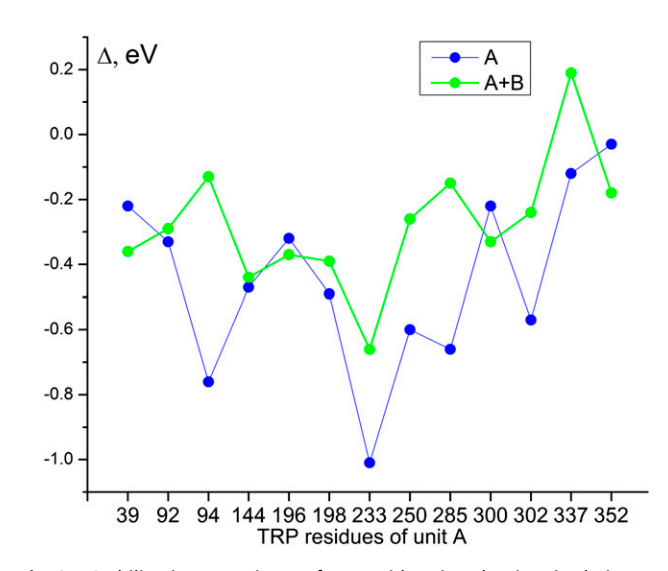


Fig. 2. Stabilization energies  $\Delta$  of Trp residues in subunit A in their  $L_a$  excited states due to charged and polar amino acid residues (AARs). Green: Electrostatic stabilization caused by AARs of the entire protein dimer. Blue: Electrostatic stabilization caused by AARs of the subunit A alone. The comparison shows that the  $L_a$  states of most Trps in subunit A are destabilized by electrostatic interaction with AARs of subunit B.

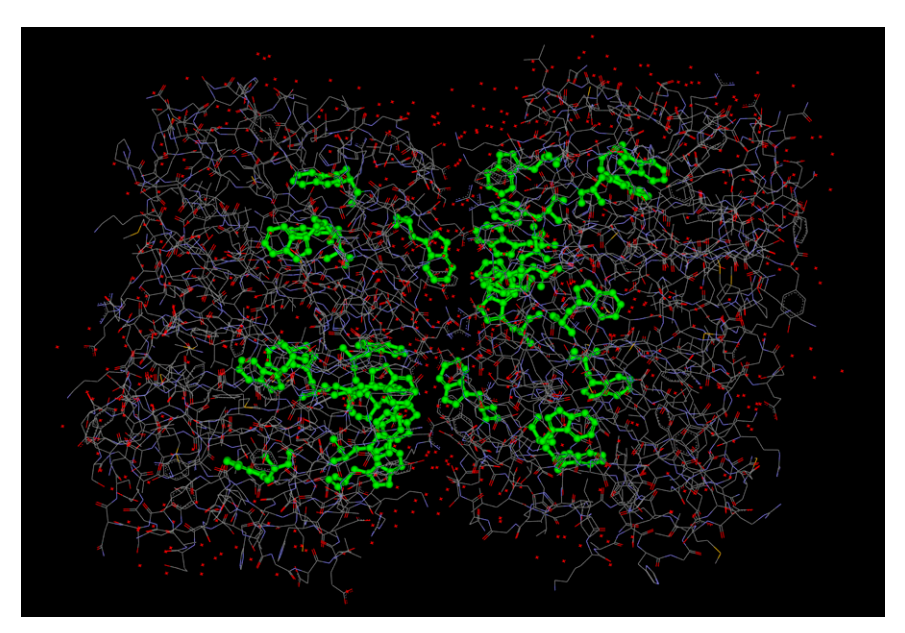


Fig. 3. UVR8 X-ray structure. Shown are Trp residues (green) in the homodimer.

electronic coupling squared. Fig. 4 shows the couplings of La and L<sub>b</sub> excited states of the Trp residues within the monomer subunit A. The coupling value depends not only on the exciton donoracceptor distance but also on the relative orientation of the Trp side chains. As can be expected from the oscillator strengths, in most cases the L<sub>b</sub>-L<sub>b</sub> coupling is weaker than the L<sub>a</sub>-L<sub>b</sub> and L<sub>a</sub>-L<sub>a</sub> couplings. The most strongly coupled chromophores form the triad cluster W233-W285-W337. The largest values of electronic couplings, 0.015 eV and 0.011 eV, are calculated for V(L<sub>a</sub>-L<sub>a</sub>) and V(L<sub>b</sub>-L<sub>a</sub>) of W233-W337, respectively. W233 is also strongly coupled with W250 and W285. More details are provided in Table S2 and Figs. S1 and S2. The favorable orientations of W233 and W94 give rise to their significant excitonic interaction, despite the relatively large interchromophore distance of ~12 Å. The reorganization energy for exciton transfer between two Trp residues can be estimated as the difference between vertical absorption and vertical emission energies (Stokes shift) of indole. For excitation energy transfer,  $\lambda(EET) = \lambda(D) + \lambda(A)$ , which gives  $2\lambda$  (indole) in our case. As the Stokes shift is also equal to  $2\lambda$ (indole),  $\lambda$ (EET) is defined by the difference of vertical absorption and vertical emission energies, which is estimated to be 0.35 eV (21). Using the EET parameters listed in Tables S1 and S2, one obtains the rates 2.70 ps<sup>-1</sup> and 0.07 ps<sup>-1</sup> for EET from W250 to W233 and from W198 to W233, respectively. It is this funneling transfer mechanism of excitation energy to the special tryptophan at the position 233 that paves the road for experimentally accessing the dynamics in fluorescence measurements (19).

Photoinduced Charge Separation Within the Triad W233-W285-W337. The residue W285 has two neighbors, W233 and W337, at short distances, 4.7 Å and 3.6 Å, respectively. The relative position of the indole groups in the triad is shown in Fig. 5. As can be seen, the indole rings of W233 and W285 are perpendicular to each other, whereas those of W285 and W337 form a  $\pi$ -stack. The results of MS-CASPT2 calculations are listed in Tables 2 and 3.

The excited-state properties of the dyads W233-W285 and W285-W337 are found to be quite different. The two first excited states, 1 and 2, of W233-W285 correspond to combinations of the indole  $L_b$  states. They are quite delocalized in the  $S_1$  state, where 72% of the exciton resides on W233 and 28% on W285; the reverse ratio is observed for the  $S_2$  state. The states 3 and 4

correspond to the La states of W285 and W233. In the CT state 5, 0.96 e is transferred from W285 to W233 (Fig. S3), leading to a large dipole moment of 18.03 D. Because of the small oscillator strength, F = 0.001, this state is hardly populated by direct excitation of the ground state. However, if we excite the system to the state L<sub>a</sub>, this localized state is expected to undergo a relatively rapid transition into the lower CT state. Using the Onsager formula  $E_{\text{solv}} = ((\varepsilon - 1)/(2\varepsilon + 1))(\mu^2/a^3)$  as a rough approximation, one can estimate the solvation energy of the CT state in unrelaxed (with only the electronic polarization being accounted for,  $\varepsilon = 2$ ) and relaxed ( $\varepsilon = 6$ ) protein environments. Taking for the cavity radius for the dimer a = 4 Å, one obtains for the CT state ( $\mu = 18 \text{ D}$ )  $E_{\text{soly}} = 0.63 \text{ eV}$  and 1.13 eV for  $\varepsilon = 2$  and  $\varepsilon = 6$ , respectively. In summary, whereas in the isolated dyad W233-W285, the CT state is calculated to be  $\sim 0.5$  eV higher than the L<sub>a</sub> state, the CT state is strongly stabilized by the protein matrix that favors the charge separation process L<sub>a</sub>→CT on energy grounds.

Also, there exists an alternative CT state, [W233<sup>+</sup> W285<sup>-</sup>] with the inverse direction of charge separation. The MS-CASPT2 calculation of the isolated dimer predicts, however, that the energy of such a state should be at least 1 eV higher than that of [W233<sup>-</sup> W285<sup>+</sup>]. Because of that result, we consider in this paper exclusively the [W233<sup>-</sup> W285<sup>+</sup>] CT state. However, we are aware that the interaction of the high-energy state [W233<sup>+</sup> W285<sup>-</sup>] with the protein environment can stabilize this radical ion pair significantly. To assess the role of the "inverted" CT state advanced models have been developed at present.

Table 2. MS-CASPT2 calculation of excited-state properties of the isolated W233-W285 dyad using the ANO-S basis and the active space (12, 12)

			Exciton		Charges	
Transition	E, eV	F	W233	W285	W233	W285
1	5.079	0.038	0.722	0.278	-0.024	0.024
2	5.112	0.052	0.255	0.745	-0.025	0.025
3	5.294	0.195	0.080	0.920	-0.029	0.029
4	5.382	0.228	0.987	0.013	-0.016	0.016
5	5.851	0.001			-0.957	0.957

Voityuk et al. PNAS Early Edition | 3 of 6

Table 3. MS-CASPT2 calculation of excited-state properties of the isolated W285-W337 dyad using the ANO-S basis and the active space (12, 12)

			Exciton		Charges	
Transition	E, eV	F	W285	W337	W285	W337
1	4.852	0.239	0.976	0.024	-0.010	0.010
2	4.919	0.128	0.073	0.927	-0.003	0.003
3	5.028	0.224	0.225	0.775	-0.000	0.000
4	5.098	0.160	0.744	0.256	-0.008	0.008
5	6.854	0.018	0.021	0.979	0.002	-0.002
6	6.877	0.031	0.976	0.024	0.007	-0.007
7	7.490	0.000	0.492	0.508	-0.001	0.001
CT*						

<sup>\*</sup>The energy of the charge transfer (CT) state is exceeding 7.5 eV as this state is not showing up within eight low-lying electronic states.

We note in passing that the absorption peak of Trp at about 300 nm corresponds to the excitation energy 4.14 eV, which is sufficient to oxidize or reduce nearby species such as aromatic amino acid residues or the protein backbone (24, 25). However, we assume that the redox reaction involving two Trps is easier to achieve than other electron transfer reactions within this protein structure. This assumption is supported by experimental mutagenic evidence (see below). Conversely, the charge recombination reaction [W233 $^-$ W285 $^+$ ]  $\rightarrow$  [W233,W285] is expected to be in the Marcus inverted region and one might have to invoke the quantum equivalent of the Marcus equation that takes into account the role of the high-frequency modes as energy acceptors (26).

Using the generalized Mulliken-Hush (GMH) (27) and fragment charge difference (FCD) (28, 29) methods, we estimated electronic couplings for the charge separation reaction in the dyad W233-W285 on the basis of the MS-CASPT2 calculations. The couplings of the first La state and the CT state in this Trp dyad system found with the GMH and FCD methods are 0.057 eV and 0.049 eV, respectively. Smaller values are obtained for the couplings of the second La state and the CT state, 0.023 eV and 0.024 eV. The corresponding rates for charge separation calculated with reorganization energy of 1 eV are found to be 2.0 ps<sup>-1</sup> and 1.1 ps<sup>-1</sup>, using the estimated free energies of -0.43 eV and -0.53 eV and not accounting for relaxation of the protein matrix. The  $\pi \rightarrow \pi^*$  excitations were also calculated for the dyad W285-W337 (Table 3). The four lowest excited states are found within the range of 0.25 eV, exhibiting relatively high oscillator strength. These states are formed by superposition of La and Lb states. No electronic states with significant charge separation showing excitation energies <7.5 eV have been identified. This result suggests that charge separation between W285 and W337 should be energetically prohibited in the UVR8 protein.

Electrostatic Effects of the Charge Transfer State. The formation of the CT state [W233<sup>-</sup> W285<sup>+</sup>] drives the dissociation of UVR8 into its subunits by breaking the salt bridges between them. Generally (17, 18) salt bridges are broken as the result of quaternary structural transitions. If so in UVR8, such structural changes have to be triggered by the large dipole moment of the CT state.

In the following, we consider a more local route to salt-bridge breaking in UVR8 and ask whether the CT state may significantly change the electrostatic potential at a salt bridge (Fig. 1), thereby giving rise to a proton transfer process within the bridge. Proton transfer from the positively charged guanidine group of Arg to the negatively charged carboxylic group of Asp (or Glu) will generate two neutral species and break the salt bridge.

Accurate theoretical models of proton transfer in proteins have been developed (30–33). For a simple and rough estimate of differences in the free energy barrier for proton transfers (34) from Arg<sup>+</sup> to Asp<sup>-</sup> we consider an expression for the reaction free energy barrier, adapted from electron transfer theory,  $(\Delta G^0 + \lambda)^2/4\lambda$ , where  $\Delta G^0$  is the standard free energy of the proton transfer reaction and  $\lambda$  is the equivalent "reorganization energy" (35). The vertical free energy difference calculated for the reactants at their initial configuration going to the products without changing the nuclear configuration is  $(\Delta G^0 + \lambda)$ . There, in comparing different reactions as in Table S3, we take  $\lambda$  to be approximately constant and assume that the main changes occur in the  $\Delta G^0$  values. Then, a major contribution to this quantity is the molecular electrostatic potential (MEP) at the final proton position minus that at its initial position. Thus, the probability of proton transfer is determined by the difference of electrostatic potential  $\Delta \varphi$  at the proton donor and the proton acceptor sites. According to our estimates compiled in Table S3, the formation of the charge-separated state leads to significant modulation of  $\Delta \varphi$  on the salt bridges between the units A and B. A positive value of the difference  $\Delta \varphi(N) - \Delta \varphi(O)$  facilitates the proton transfer from Arg+ to Asp- and stabilizes the neutral amino acid residues.

We note that the CT state of Trp233 and Trp285 is stabilized by its environment due to electronic polarization of the protein environment. This effect counteracts its unfavorable interaction with the charged residues R146, R286, R338, R354, D44, D96, D107, E53, and E182. The largest difference in MEP, i.e., 1.2 eV, is calculated for the ionic bridge R286-D96. Because of proton transfer from R286 to D96, also the electrostatic interaction R286-D107 becomes significantly smaller. We are aware that pK<sub>a</sub> values of Arg and Asp are quite different, 12.1 and 3.7, respectively. A change in the electrostatic potential on N (Arg) and O (Asp) required to transfer the proton from Arg to Asp at T = 300 K can be estimated as  $\Delta \varphi(eV) \approx 0.06 \cdot \Delta pK_a$ , which gives  $\Delta \varphi = 0.50$  eV. According to our data (Table S3), the change in the electrostatic potential for R286-D96 due to the formation of the charge transfer state is 1.2 eV, which would be more than enough to initiate the proton shift from R286 to D96.

To initiate the dissociation reaction by a change of the electrostatic potential, the lifetime of the CT state has to be sufficiently long. If we assume that the lifetime of the CT state is no longer than a few nanoseconds, during this time the proton transfer within the salt bridges should occur together with the

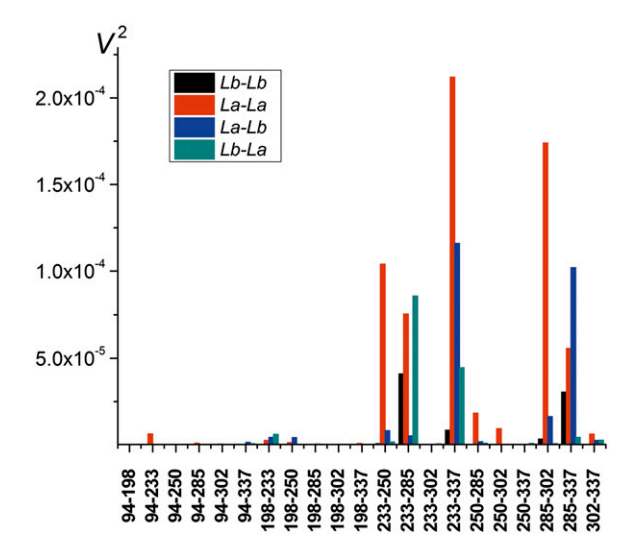


**Fig. 4.** Excitonic coupling of Trp residues in subunit A in their  $L_a$  and  $L_b$  excited states.

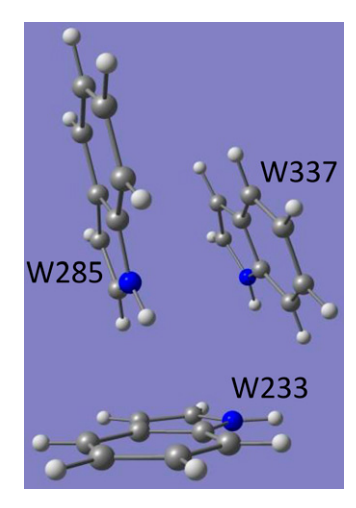


**Fig. 5.** Relative position of indoles in the triad W233-W285-W337 encoding C in gray, H in white, and N in blue.

corresponding changes in the orientation of the Arg and Asp residues. We assume also that the orientational transformation following the proton transfer prohibits the immediate back transfer of the proton after recombination of the charge-separated state [W233<sup>-</sup>-W285<sup>+</sup>]. Then, dissociation of UVR8 into its monomers would become feasible.

Comparison of Calculated and Experimental Results. Experimentally the potential involvement of different tryptophans in the important triad W285-W233-W337 has been studied by site-specific mutagenesis (8–10, 19). Our discussion below is focused on purified in vitro proteins for which X-ray structural analysis has proved that mutations did not impair their structural integrity.

**W285F.** The phenylalanine mutant W285F forms a constitutive dimer that fails to respond to UV-B light as concluded from circular dichroism (8) and fluorescence spectroscopy (9). We note in passing that this dimeric mutant when expressed in yeast is nonfunctional because it does not monomerize in response to UV-B radiation (10). In plants UV-B light does not give rise to gene expression and as a consequence these mutated plants are highly sensitive to UV-B-induced damaging (7). The failure of the W285F mutant is in line with our calculations. The replacement of Trp by Phe at position 285 is expected to prevent the formation of the charge-separated state. In our mechanism, however, it is the [W233--W233+] radical ion pair state that is instrumental for the breakage of salt bridges that stabilize the dimer structure. By the same argument, the failure of function of this W285F mutant is consistent with the notion that other redox species—for instance, the amides (22, 24, 36, 37) of the protein backbone or, although less probable, the arginines (8)—do hardly substitute as redox partners. Also in line with our mechanism is the recently reported drastic increase of both the fluorescence lifetime and the steady-state quantum yield of Trp in the dimeric mutant W285F of the isolated UVR8 protein compared with its wild type (8). These fluorescence experiments confirm also in a most convincing way the funneling of the excitation energy to the redox active Trp233.

*W233F.* This mutation leads to the loss of response to UV-B radiation similarly to that in the mutant W285F (8, 9). Following our calculations, this failure is not surprising due to the double role of W233 as both excitation energy sink in the excitonic coupling scheme of the Trp cluster and electron acceptor giving rise to the radical ion pair state [W233<sup>-</sup> W285<sup>+</sup>].

*W337F.* In contrast to mutations of W285F and W233F that are in wild-type UVR8 involved in intertryptophan electron transfer, mutation of W337 to phenylalanine shows less effect. Apart from a reduced response to UV-B light, this mutant still maintains the UV-B induced dimer-to-monomer conversion (8). This behavior is in line with our mechanism that considers the two tryptophans W285 and W233 as the main players in the induction of the dissociation process of the dimer UVR8 upon exposure to UV-B.

#### **Conclusions**

On the basis of high-level MS-CASPT2 quantum-mechanical calculations we suggest a plausible mechanism (Fig. 6) for the dissociation of the UVR8 homodimer upon UV-B photoreception. Electronic interactions, directionality, and probability of excitation energy transfer between the Trp chromophores of the homodimer have been analyzed together with the functionally important role of the triad Trp233-Trp285-Trp337 at the interface of the two monomer units. It is shown that the strong electrostatic stabilization of the L<sub>a</sub> excited state of Trp233 by the protein matrix makes this tryptophan energetically favorable for excitons to flow from other Trps into this "sink" at position 233. Then, a fast decay (on the picosecond timescale) of the excited state via charge separation into the radical ion pair Trp285(+)-Trp233(-) generates a large dipole moment of ~18 D. Thereby, according to our calculations the electrostatic interaction between the monomeric subunits caused by dimer-stabilizing salt bridges is weakened and so the dissociation of the dimer is facilitated. However, we emphasize that the large dipole moment of the CT state could as well induce changes in the quaternary protein structure that lead to the breaking of the salt bridges and thus to the dissociation of the dimer. The mechanism depicted in Fig. 6 can explain the experimental results from mutagenesis of UVR8, which show that replacement of either key residue, Trp285 or Trp233, by phenylalanine inhibits the photodissociation of UVR8. In summary, our calculations support the notion that the two tryptophans, Trp285 and Trp233, are indeed the key amino acid residues responsible for both the accumulation of excitons at Trp233 and the subsequent charge separation between Trp233 and Trp285. The resulting large dipole moment leads to the breaking of the dimer-stabilizing salt bridges and starts with the signal chain of the UV-B sensor UVR8.

#### Methods

Quantum chemical calculations as well as the estimation of electrostatic interactions are based on the experimental X-ray structure (9) of the UVR8 protein (Protein Data Bank ID: 4DNW). The MS-CASPT2 calculations (38) were performed with MOLCAS 7.6, using the ANO-S and ANO-L basis sets (39). The active space (10, 10) comprising 10 electrons distributed among 10  $\pi$  orbitals was used to calculate excited-state properties of indole. Excitonic couplings of excited states of Trps were computed using the transition densities for both the  $L_a$  and  $L_b$  excited states of indole. For complexes [Trp233, Trp285] and [Trp285, Trp337] only the side chains (indole moieties) were included in the model; in this case the active space (12, 12) was used.

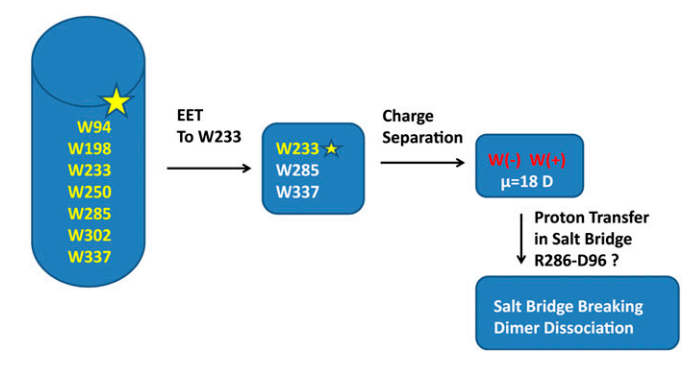


Fig. 6. Primary photoprocesses in UVR8.

Voityuk et al. PNAS Early Edition | 5 of 6

$$k_{\text{EET}} = \frac{2\pi}{\hbar} V^2(\text{FCWD}),$$
 [1]

that accounts for the overlap of vibrational states of donor and acceptor and can be approximately estimated using the classical Marcus equation (40),

$$(FCWD) = (4\pi\lambda kT)^{-1/2} \exp\left[\frac{-\left(\Delta G^0 + \lambda\right)^2}{4\lambda kT}\right],$$
 [2]

where  $\lambda$  is the reorganization energy and  $\Delta G^0$  is the standard free energy change of the process. In the case of EET,  $\Delta G^0$  is to a good approximation equivalent to  $\Delta E$ , i.e., the energy difference of the donor and acceptor sites. This approach to calculate the rate of excitation energy transfer was used in several previous studies (41, 42). The EET rate and its distance dependence are controlled by the electronic coupling of the corresponding diabatic states,  $k_{\text{EET}}(\text{Trp}_I \rightarrow \text{Trp}_J) \sim V_{IJ}^2$ . In line with Förster theory, excitonic coupling of two singlet excited state of molecules A and B is estimated as the interaction of their transition dipole moments  $\mu_A$  and  $\mu_{Br}$  $V_{dd} = (\mu_A \cdot \mu_B)/R_{AB}^3 - (3(\mu_A \cdot R_{AB})(\mu_B \cdot R_{AB})/R_{AB}^5)$ , where  $R_{AB}$  is the intermolecular

- 1. Kliebenstein DJ, Lim JE, Landry LG, Last RL (2002) Arabidopsis UVR8 regulates ultraviolet-B signal transduction and tolerance and contains sequence similarity to human regulator of chromatin condensation 1. Plant Physiol 130(1):234-243.
- 2. Kaiserli E, Jenkins GI (2007) UV-B promotes rapid nuclear translocation of the Arabidopsis UV-B specific signaling component UVR8 and activates its function in the nucleus. Plant Cell 19(8):2662-2673.
- 3. Jenkins GI (2009) Signal transduction in responses to UV-B radiation. Annu Rev Plant Biol 60:407-431
- 4. Brown BA, et al. (2005) A UV-B-specific signaling component orchestrates plant UV protection. Proc Natl Acad Sci USA 102(50):18225-18230.
- 5. Tong HY, et al. (2008) Role of root UV-B sensing in Arabidopsis early seedling development. Proc Natl Acad Sci USA 105(52):21039-21044.
- 6. Heijde M, Ulm R (2012) UV-B photoreceptor-mediated signalling in plants. Trends Plant Sci 17(4):230-237.
- 7. O'Hara A, Jenkins GI (2012) In vivo function of tryptophans in the Arabidopsis UV-B photoreceptor UVR8. Plant Cell 24(9):3755-3766.
- 8. Christie JM, et al. (2012) Plant UVR8 photoreceptor senses UV-B by tryptophanmediated disruption of cross-dimer salt bridges. Science 335(6075):1492-1496.
- 9. Wu D, et al. (2012) Structural basis of ultraviolet-B perception by UVR8. Nature 484(7393):214-219.
- 10. Rizzini L, et al. (2011) Perception of UV-B by the Arabidopsis UVR8 protein. Science 332(6025):103-106.
- 11. Fritsche E, et al. (2007) Lightening up the UV response by identification of the arylhydrocarbon receptor as a cytoplasmatic target for ultraviolet B radiation. Proc Natl Acad Sci USA 104(21):8851-8856.
- 12. Brown BA, Headland LR, Jenkins GI (2009) UV-B action spectrum for UVR8-mediated HY5 transcript accumulation in Arabidopsis, Photochem Photobiol 85(5):1147-1155.
- 13. Cloix C, et al. (2012) C-terminal region of the UV-B photoreceptor UVR8 initiates signaling through interaction with the COP1 protein. Proc Natl Acad Sci USA 109(40): 16366-16370.
- 14. Heijde M, Ulm R (2013) Reversion of the Arabidopsis UV-B photoreceptor UVR8 to the homodimeric ground state. Proc Natl Acad Sci USA 110(3):1113-1118.
- 15. Gruber H, et al. (2010) Negative feedback regulation of UV-B-induced photomorphogenesis and stress acclimation in Arabidopsis. Proc Natl Acad Sci USA 107(46): 20132-20137.
- 16. Crefcoeur RP. Yin R. Ulm R. Halazonetis TD (2013) Ultraviolet-B-mediated induction of protein-protein interactions in mammalian cells. Nat Commun 4:1779.
- 17. Cui O. Karplus M (2008) Allostery and cooperativity revisited. Protein Sci 17(8): 1295-1307.
- 18. Mithu VS, et al. (2011) Zn(++) binding disrupts the Asp(23)-Lvs(28) salt bridge without altering the hairpin-shaped cross- $\beta$  Structure of A $\beta$ (42) amyloid aggregates. Biophys J 101(11):2825-2832.
- 19. Liu Z, et al. (2014) Quenching dynamics of ultraviolet-light perception by UVR8 photoreceptor. J Phys Chem Lett 5(1):69-72.
- 20. Wu M. Strid A. Eriksson LA (2013) Interactions and stabilities of the UV RESISTANCE LOCUS8 (UVR8) protein dimer and its key mutants. J Chem Inf Model 53(7): 1736-1746.
- 21. Giussani A, Merchan M, Roca-Sanjuan D, Lindh R (2011) Essential on the photophysics and photochemistry of the indole chromophore by using a totally unconstrained theoretical approach. J Chem Theory Comput 7(12):4088-4096.
- 22. Callis PR (1997) 1La and 1Lb transitions of tryptophan: Applications of theory and experimental observations to fluorescence of proteins. Methods Enzymol 278:
- 23. Dolinsky TJ, et al. (2007) PDB2PQR: Expanding and upgrading automated preparation of biomolecular structures for molecular simulations. Nucleic Acids Res 35(Web Server issue):W522-W555

distance. This expression provides good estimates when the spatial extension of the transition densities in the molecules is much smaller than the distance  $R_{AB}$ . More accurate values of the excitonic coupling can be obtained using transition atomic charges (43):

$$V_{tc} = \sum_{\substack{i \in A \\ i \in B}} \frac{q_i \ q_j}{R_{ij}}.$$
 [3]

In Eq. 3,  $q_i$  and  $q_i$  are transition charges derived from quantum mechanical calculations of excited states of the molecules, and i and j are summed over all atoms of the molecules A and B. The performance of the transition charge model was recently discussed (44).

ACKNOWLEDGMENTS. The authors thank Lars-Oliver Essen for bringing the protein UVR8 in all its aspects to their knowledge. The authors thank William W. Parson for critically reading the manuscript and for many constructive comments. A.A.V. thanks the Ministry of Science and Innovation of Spain for financial support under Grant CTQ 2011-26573. R.A.M. thanks the Office of Naval Research and the Army Research Office for the support of his research. This work was generously supported by the Nanyang Technological University (M.-E.M.-B.).

- 24. Qiu W, et al. (2008) Ultrafast quenching of TRP fluorescence in proteins: Interresidue and intrahelical electron transfer. Chem Phys 350(1-3):154-164.
- 25. Muiño PL, Callis PR (2009) Solvent effects on the fluorescence quenching of tryptophan by amides via electron transfer. Experimental and computational studies. J Phys Chem B 113(9):2572-2577.
- 26. Kestner NR, Logan J, Jortner J (1974) Thermal electron transfer reactions in polar solvents. J Phys Chem 78(21):2148-2166.
- 27. Cave RJ. Newton MD (1997) Calculation of electronic coupling matrix elements for ground and excited state electron transfer reactions: Comparison of the Generalized Mulliken-Hush and block diagonalization methods. J Chem Phys 106(22):9213-9226.
- 28. Voityuk AA, Rösch N (2002) Fragment charge difference method for estimating donor-acceptor electronic coupling. Application to DNA  $\pi$ -stacks. J Chem Phys 117(12): 5607-5616.
- 29. Voityuk AA (2013) Estimation of electronic coupling for photoinduced chargeseparation and charge recombination using the fragment charge difference method. J Phys Chem C 117(6):2670-2675.
- 30. Xiang Y, Warshel A (2008) Quantifying free energy profiles of proton transfer reactions in solution and proteins by using a diabatic FDFT mapping. J Phys Chem B 112(3):1007-1015.
- 31. Billeter SR, Webb SP, Agarwal PK, Iordanov T, Hammes-Schiffer S (2001) Hydride transfer in liver alcohol dehydrogenase: Quantum dynamics, kinetic isotope effects, and role of enzyme motion. J Am Chem Soc 123(45):11262-11272.
- 32. Gao J, et al. (2006) Mechanisms and free energies of enzymatic reactions. Chem Rev 106(8):3188-3209.
- 33. Kretchmer JS. Miller TF. 3rd (2013) Direct simulation of proton-coupled electron transfer across multiple regimes. J Chem Phys 138(13):134109.
- 34. Marcus RA (2007) H and other transfers in enzymes and in solution: Theory and computations, a unified view. 2. Applications to experiment and computations. J Phys Chem B 111(24):6643-6654.
- 35. Kuznetsov AM, Ulstrup J (1999) Proton and hydrogen atom tunneling in hydrolytic and redox enzyme catalysis. Can J Chem 77(5-6):1085-1096.
- 36. McMillan AW, et al. (2013) Fluorescence of tryptophan in designed hairpin and Trpcage miniproteins: Measurements of fluorescence yields and calculations by quantum mechanical molecular dynamics simulations. J Phys Chem B 117(6):1790-1809.
- 37. Zhang L. Kao YT. Oiu W. Wang L. Zhong D (2006) Femtosecond studies of tryptophan fluorescence dynamics in proteins: Local solvation and electronic quenching. J Phys Chem B 110(37):18097-18103.
- 38. Finley J, Malmqvist PA, Roos BO, Serrano-Andres L (1998) The multi-state CASPT2 method. Chem Phys Lett 288(2-4):299-306
- 39. Aquilante F, et al. (2010) MOLCAS 7: The next generation. J Comput Chem 31(1): 224-247.
- 40. Marcus RA. Sutin N (1985) Electron transfers in chemistry and biology, Biochim Biophys Acta 811(3):265-322.
- 41. Subotnik JE, Vura-Weis J, Sodt AJ, Ratner MA (2010) Predicting accurate electronic excitation transfer rates via Marcus theory with Boys or Edmiston-Ruedenberg localized diabatization. J Phys Chem A 114(33):8665-8675.
- 42. Curutchet C, Voityuk AA (2011) Triplet-triplet energy transfer in DNA: A process that occurs on the nanosecond timescale. Angew Chem Int Ed Engl 50(8):1820-1822.
- 43. Chang JC (1977) Monopole effects on electronic excitation interactions between large molecules. 1. Application to energy-transfer in chlorophylls. J Chem Phys 67(9): 3901-3909.
- 44. Kistler KA, Spano FC, Matsika SA (2013) A benchmark of excitonic couplings derived from atomic transition charges. J Phys Chem B 117(7):2032-2044.